The Astrophysical Journal, 885:114 (8pp), 2019 November 10 https://doi.org/10.3847/1538-4357/ab45f8

Abundant Refractory Sulfur in Protoplanetary Disks

Mihkel Kama[1], Oliver Shorttle[1], Adam S. Jermyn[1,2], Colin P. Folsom[3], Kenji Furuya[4], Edwin A. Bergin[5], Catherine Walsh[6], and Lindsay Keller[7]
[1] Institute of Astronomy, University of Cambridge, Madingley Road, Cambridge CB3 0HA, UK; mkama@ast.cam.ac.uk
[2] Kavli Institute for Theoretical Physics, University of California at Santa Barbara, Santa Barbara, CA 93106, USA
[3] IRAP, Université de Toulouse, CNRS, UPS, CNES, F-31400, Toulouse, France
[4] Center for Computational Sciences, University of Tsukuba, 1-1-1 Tennoudai, 305-8577, Tsukuba, Japan
[5] Department of Astronomy, University of Michigan, 1085 S. University Avenue, Ann Arbor, MI 48109, USA
[6] School of Physics and Astronomy, University of Leeds, Leeds, LS2 9JT, UK
[7] ARES, Code XI3, NASA/JSC, Houston, TX 77058, USA
Received 2019 June 8; revised 2019 July 29; accepted 2019 August 12; published 2019 November 6

Abstract

Sulfur is one of the most abundant elements in the universe, with important roles in astro-, geo-, and biochemistry. Its main reservoirs in planet-forming disks have previously eluded detection: gaseous molecules only account for $<1\%$ of total elemental sulfur, with the rest likely in either ices or refractory minerals. We use a new method to measure the refractory component. Mechanisms such as giant planets can filter out dust from gas accreting onto disk-hosting stars. For stars above 1.4 solar masses, this leaves a chemical signature on the stellar photosphere that can be used to determine the fraction of each element that is locked in dust. Here, we present an application of this method to sulfur, zinc, and sodium. We analyze the accretion-contaminated photospheres of a sample of young stars and find $(89 \pm 8)\%$ of elemental sulfur is in refractory form in their disks. The main carrier is much more refractory than water ice, consistent with sulfide minerals such as FeS.

Unified Astronomy Thesaurus concepts: Planet formation (1241); Protoplanetary disks (1300); Astrochemistry (75); Meteorite composition (1037); Chemically peculiar stars (226)

1. Introduction

Sulfur is an atomic gas in the interstellar medium (ISM), but is found entirely in rocks in the inner solar system. Its main reservoir in protoplanetary disks has thus far eluded observation. We study a sample of 16 young, disk-hosting stars, listed in Appendix A. Trapping of large dust grains in their disks, evidenced by radial gaps and cavities in the distribution of millimeter-wavelength continuum emission (Andrews et al. 2009; van der Marel et al. 2016; Andrews et al. 2018), has been shown to correlate with a depletion of refractory elements like iron on the stellar surface (Kama et al. 2015). In this paper, we measure the refractory fraction of sulfur, zinc, and sodium by comparing their behavior with the overall level of dust depletion in the accreting inner disk material.

The cosmic journey of sulfur is summarized in Figure 1, where we trace sulfur from the ISM, through disks (this work), and finally into rocky and icy planetesimals. Sulfur is chiefly synthesized in Type II supernovae (e.g., Woosley & Weaver 1995; Ryde & Lambert 2005) and supernova remnants contain gas-phase molecules such as SO (Matsuura et al. 2017). In (post-)asymptotic giant branch stars, observations reveal a high abundance of gas-phase molecular carriers such as CS, SO, SiS, and H_2S, but also sulfide mineral grains such as FeS and MgS (e.g., Hony et al. 2002; Danilovich et al. 2016, 2017, 2018). Refractory sulfur is converted to gas by the enhanced sputtering rate of solid sulfide by ions, a process which is much less efficient for metals and silicates (Keller et al. 2013). Once it has entered the diffuse ISM, sulfur is entirely in the gas phase (Joseph et al. 1986; Jenkins 2009).

As sulfur moves into denser regions of the ISM, its gas-phase abundance drops to $\sim$13% of the diffuse ISM value (Jenkins 2009). Little is known about the reservoirs consuming sulfur along the path from the ISM to the denser star-forming molecular cloud cores and protoplanetary disks, in which the vast majority of it has eluded observation. Our measurement fills this gap. What was known until now is that volatile ices such as H_2S and OCS account for $\lesssim$4% of the total S inventory in star-forming cores (Geballe et al. 1985; Smith 1991; Palumbo et al. 1995; Boogert et al. 1997, 2015, Figure 1), while in shocked regions in jets from embedded protostars only 5%–10% of total sulfur is in the gas phase (Anderson et al. 2013). In planet-forming disks, gas-phase H_2S, CS, and SO only account for $\lesssim$1% of all sulfur (Dutrey et al. 1997; Wakelam et al. 2004; Fuente et al. 2010; Dutrey et al. 2011; Martín-Doménech et al. 2016; Semenov et al. 2018), while tentatively detected spectral features of FeS have suggested a poorly quantifiable refractory component (Keller et al. 2002; Lisse et al. 2007).

2. Analysis

Our analysis relies on dust trapping in disks, which removes some refractory material before it can accrete onto the central star; and on the fact that early-type stars are dominated by diffusive rather than convective mixing in their envelopes, which allows recently accreted disk material to dominate the composition of their surface. These considerations allow us to extract new information from composition data of disk-hosting stars, gathered from the literature and our own previous work.

Stars more massive than $1.4\,M_\odot$ have radiative envelopes where mixing is dominated by slow diffusion, as opposed to the faster convective mixing which occurs in lower-mass stars. Their observable photosphere mass, of order $10^{-10}\,M_\odot$, can be entirely replaced on a timescale of days at disk accretion rates $\dot{M}_{\rm acc} \sim 10^{-8}$ to $10^{-7}\,M_\odot\,{\rm yr}^{-1}$ (Jermyn & Kama 2018). Measuring the stellar surface composition is thus a tool for studying the elemental composition of material recently accreted from a

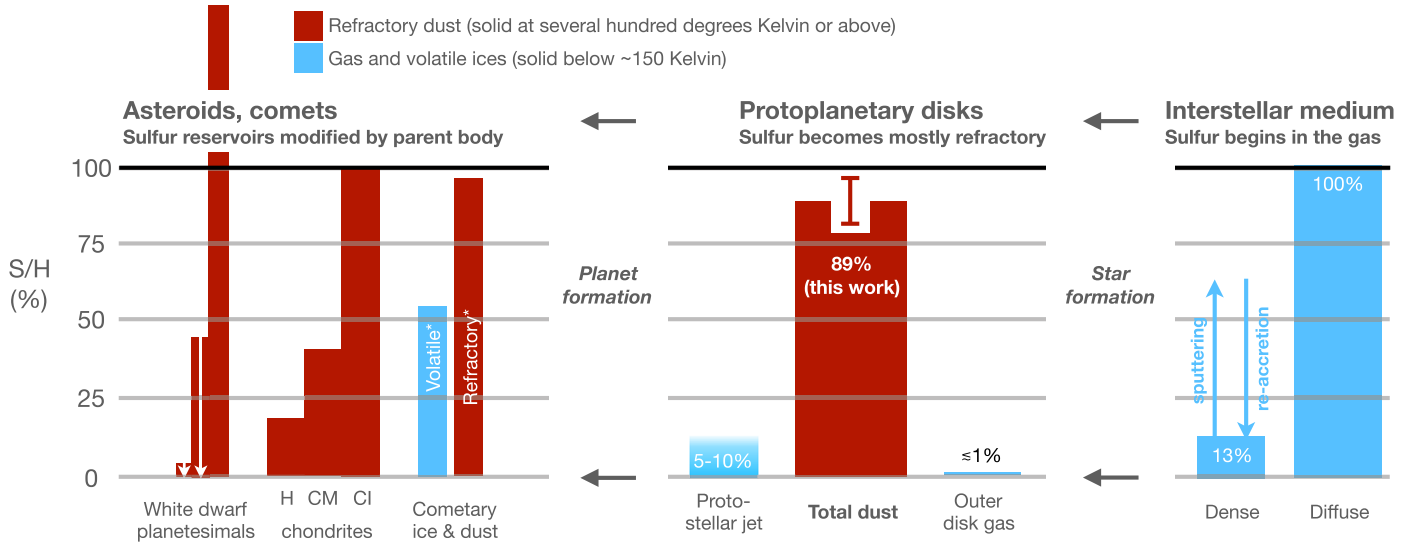

Figure 1. Fractional importance of volatile (blue) and refractory (red) reservoirs of sulfur, as measured in environments sampling different stages of the star and planet formation process (Wasson & Kallemeyn 1988; Dutrey et al. 1997; Wakelam et al. 2004; Jenkins 2009; Fuente et al. 2010; Dutrey et al. 2011; Gänsicke et al. 2012; Anderson et al. 2013; Xu et al. 2013, 2017; Calmonte et al. 2016; Martín-Doménech et al. 2016). The normalizations of the panels are, from right to left, the highest, super-solar gas-phase abundance in the diffuse ISM (Jenkins 2009); the reference sulfur abundance in early-type stars as determined from young open clusters (Fossati et al. 2011; Martin et al. 2017); and solar S/H, to which we scale via silicon for dust and oxygen for ices (Asplund et al. 2009), assuming refractories have a solar abundance of Si and cometary ices have solar O. White arrows covering solid bars indicate upper limits.

circumstellar disk (the Contaminated A-stars Method, CAM; Kama et al. 2015; Jermyn & Kama 2018). Surface layers built up on the star from dust-depleted material in the protoplanetary disk stage form a small fraction of the total mass of the star, and are lost through diffusive and rotational mixing with the bulk of the star within a million years after the disk dissipates (Jermyn & Kama 2018).

2.1. Stellar Surface and Inner Disk Composition

We gathered surface elemental composition data for a sample of 16 young, disk-hosting stars of stellar spectral type B9 through F4 from the literature (Folsom et al. 2012; Kama et al. 2016, see Appendix A for details). We assume each star and disk starts out with the same reference composition $(\mathrm{X/H})_{\mathrm{ref}}$, where X is an element, for which we adopted the mean abundances from studies of nearby, young open clusters by Martin et al. (2017, NGC 6250, age 26 Myr) and Fossati et al. (2011, NGC 5460, age 158 Myr).[8] All elemental abundance trends we report and analyze below are present in the disk-hosting star sample alone, but the robustness is increased by using a reference set of disk-free stars. This also gives us enough data to discard disk hosts with poorly quantified errorbars.

A parcel of material in a disk starts out with a fraction f_{X} of each element X in the refractory (dust grains) component and the rest in volatiles (gas, ice). For hydrogen $f_{\mathrm{H}} = 0$ and for strong refractories such as iron and titanium we fix $f_{\mathrm{Fe,Ti}} = 1$, expecting them to be entirely refractory and essentially measuring the overall level of dust depletion in the inner disk. For each star, we follow Jermyn & Kama (2018) and Section 2.4 in calculating the mixing fraction $f_{\mathrm{ph}} \in [0, 1]$ of recently accreted material. The results below are not substantially different if we assume the photosphere is totally replaced by recent accretion in all the stars ($f_{\mathrm{ph}} = 1$). Each star–disk system also has a dust depletion fitting parameter, δ_{dust}, which scales the refractory component of each element to account for dust retained in the disk. The abundance of X in disk material that makes it onto the star is $(\mathrm{X/H})_{\mathrm{disk}}$. We perform statistical inference to obtain f_{X} for O, S, Zn, and Na using Equations (1) and (2). Appendix A describes the disk-hosting and reference stars, and Section 2.4 the inference model relating the measured composition of accreting stars to the inner disk material.

In order to, first, test our results for robustness and, second, to consider zinc for which all open cluster stars failed the quality criteria, we also ran our analysis using the solar composition from Asplund et al. (2009). We note that the solar composition is not an optimal reference for the early-type star abundances, which were determined using a different set of spectral features and stellar atmospheric models, and may be further modulated by Galactic chemical evolution. We have made no attempt in this work to quantify these confounding effects, focusing in our main analysis on the direct comparison of open cluster and disk-hosting early-type stars.

2.2. Dust Trapping as a Chemical Isolation Tool

Our method is insensitive to the precise mechanism of dust trapping in disks, but segregation of some dust from a parcel of disk material generally requires a radially non-monotonous midplane gas pressure. Trapping is evidenced by resolved observations which show millimeter-sized grains adjacent to dust-poor regions (e.g., Andrews et al. 2009; van der Marel et al. 2016; Andrews et al. 2018). Such dust cavities and gaps in disks correlate with a lowered abundance of refractory elements accreted onto the central star (Kama et al. 2015) and planet-induced dust traps match the observations (Pinilla et al. 2012). A planet embedded in a protoplanetary disk causes a pressure bump to form radially outward of the planet (Figure 2); gas drag and centrifugal forces then conspire to

[8] Even though the open cluster early-type stars themselves have measurement scatter of a few tenths of dex, the disk-hosting stars which have dust gaps or cavities have surface abundances of refractory elements extending well below this range.

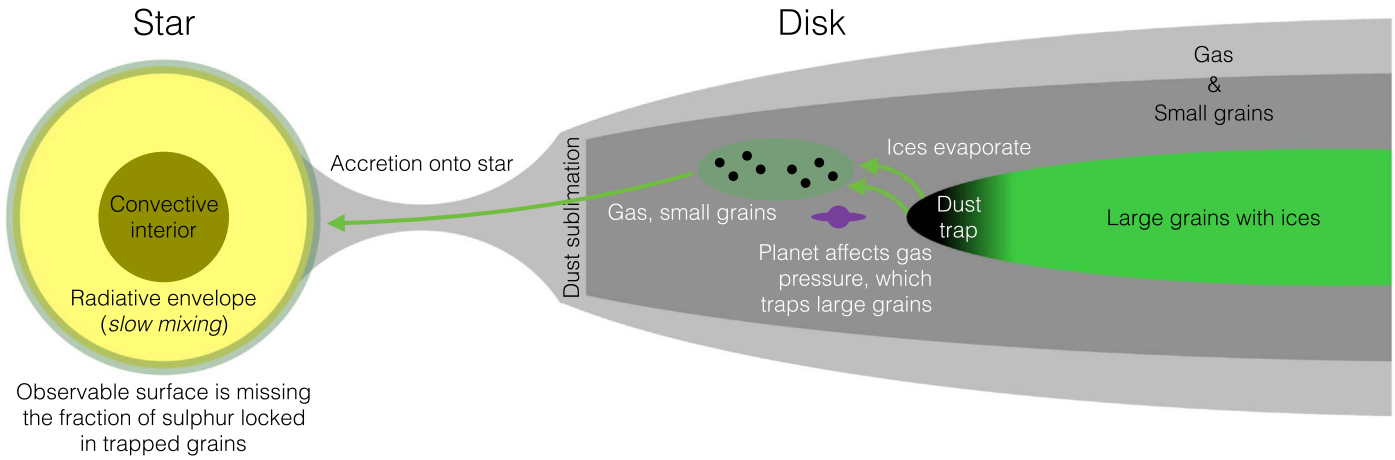

Figure 2. Accretion of gas, ice, and dust grains from a disk onto a young star. While gas and smaller dust grains flow freely toward the star, a radial gas pressure bump, potentially induced by a planet, filters away the larger dust grains. This prevents some dust from moving inwards and accreting, depriving material reaching the star of refractory elements. The chemical signature is visible in the photosphere of stars more massive than 1.4 $M_{\odot}$, which lack a convective envelope, as long as the dust trap exists and material from that disk region is reaching the star.

Table 1
Measured Photospheric Abundances of O, S, Zn, Na, Fe, and Ti from Folsom et al. (2012) for Our Sample Stars Except HD 100546, which Is from Kama et al. (2016)

Star	$\log_{10}\left(\frac{\mathrm{O}}{\mathrm{H}}\right)$	$\log_{10}\left(\frac{\mathrm{S}}{\mathrm{H}}\right)$	$\log_{10}\left(\frac{\mathrm{Zn}}{\mathrm{H}}\right)$	$\log_{10}\left(\frac{\mathrm{Na}}{\mathrm{H}}\right)$	$\log_{10}\left(\frac{\mathrm{Fe}}{\mathrm{H}}\right)$	$\log_{10}\left(\frac{\mathrm{Ti}}{\mathrm{H}}\right)$	$\log_{10}(f_{\mathrm{ph}})$
HD 31648	-3.24 ± 0.05[a]	-4.456 ± 0.30[a]	⋯	-5.68 ± 0.25[a]	-4.43 ± 0.13	-6.78 ± 0.09	-6.680×10^{-3}
HD 36112	-3.14 ± 0.10[a]	-4.75 ± 0.16[a]	-7.76 ± 0.40[a]	-5.54 ± 0.15[a]	-4.45 ± 0.14	-6.94 ± 0.20	-6.771×10^{-3}
HD 68695	-3.13 ± 0.10	-4.56 ± 0.30[a]	⋯	-6.16 ± 0.40[a]	-5.12 ± 0.22	-7.67 ± 0.25	-6.784×10^{-3}
HD 100546	-3.25 ± 0.10	-5.37 ± 0.50[a]	⋯	⋯	-5.67 ± 0.08	-8.12 ± 0.23	-6.904×10^{-3}
HD 101412	-3.08 ± 0.09	-4.92 ± 0.12	⋯	-5.52 ± 0.15[a]	-5.04 ± 0.19	-7.71 ± 0.23	-6.713×10^{-3}
HD 139614	-3.29 ± 0.10[a]	-5.14 ± 0.15	-8.26 ± 0.30[a]	-6.10 ± 0.12	-5.03 ± 0.13	-7.47 ± 0.14	-6.696×10^{-3}
HD 141569	-3.01 ± 0.10	⋯	⋯	$\leqslant -5.16$	-5.21 ± 0.32	-7.70 ± 0.32	-4.141×10^{-1}
HD 142666	-3.14 ± 0.15[a]	-4.66 ± 0.15	-7.86 ± 0.30[a]	-5.73 ± 0.15[a]	-4.80 ± 0.11	-7.35 ± 0.20	-3.071×10^{-1}
HD 144432	-3.13 ± 0.10[a]	-4.78 ± 0.05	-7.53 ± 0.20	-5.82 ± 0.09	-4.66 ± 0.09	-7.22 ± 0.16	-5.114×10^{-1}
HD 163296	-3.27 ± 0.15	⋯	⋯	-5.56 ± 0.50[a]	-4.35 ± 0.15	-6.88 ± 0.10	-4.178×10^{-1}
HD 169142	-3.34 ± 0.13	-5.06 ± 0.12	-8.67 ± 0.08[a]	-6.14 ± 0.08[a]	-5.09 ± 0.11	-7.61 ± 0.10	-3.525×10^{-1}
HD 179218	-3.06 ± 0.13	-4.16 ± 0.40[a]	⋯	-5.46 ± 0.30[a]	-4.99 ± 0.13	-7.53 ± 0.12	-6.804×10^{-3}
HD 244604	-3.19 ± 0.08	-4.44 ± 0.15[a]	⋯	-5.36 ± 0.30	-4.31 ± 0.24	-6.77 ± 0.31	-7.291×10^{-1}
HD 245185	-3.13 ± 0.17	⋯	⋯	⋯	-5.23 ± 0.33	-7.89 ± 0.38	-6.848×10^{-3}
HD 278937	-3.37 ± 0.05	-4.79 ± 0.14	$\leqslant 7.96$	-6.26 ± 0.30[a]	-5.08 ± 0.16	-7.77 ± 0.10	-6.928×10^{-3}
T Ori	-3.12 ± 0.12	-4.06 ± 0.30[a]	⋯	-6.06 ± 0.30[a]	-4.94 ± 0.10	-7.51 ± 0.17	-4.437×10^{-1}
Reference (ref)	-3.33 ± 0.07	-4.33 ± 0.28	…	-5.86	-4.65 ± 0.47	-7.10 ± 0.62	
Solar ($\odot$)	-3.31 ± 0.05	-4.88 ± 0.03	-7.44 ± 0.05	-5.76 ± 0.04	-4.50 ± 0.04	-7.05 ± 0.05	

Notes. The reference abundances are the mean of open cluster stars (with errors which are the sample standard deviation), except for zinc which is referenced to the Asplund et al. (2009) solar value ($^{\odot}$). The photospheric contamination fraction was calculated for each star following Jermyn & Kama (2018).
[a] Marks abundances determined from a single spectral feature or a very limited spectral range—these values are excluded from our fitting but shown in all plots as lighter-colored symbols.

accumulate larger dust particles in the local pressure maximum (Pinilla et al. 2012; Birnstiel et al. 2016). As large grains dominate the dust mass, trapping has a major effect on the total elemental composition of the disk material that reaches the star (Kama et al. 2015). Building on the relation between stellar photospheric compositions and dust disk structure, we can open a new window onto the reservoirs of each element in the zone of terrestrial planet formation.

2.3. Volatile, Refractory, and Intermediate Elements

The observed surface compositions of our compiled sample of disk-hosting stars and the open cluster reference are given in Table 1. We use the analysis described in Section 2.4 and stellar parameters summarized in Table 2 to infer the elemental composition of the inner disk for the accreting, young stars. These inferred abundances are shown alongside the open cluster reference in Figure 3, to illustrate the volatile behavior of oxygen, the refractory behavior of titanium and iron, and the behavior of sulfur. We show correlation plots of iron (50% condensation temperature $T_{\mathrm{c}} = 1334$ K, Lodders 2003) with sulfur (664 K), oxygen (180 K), and titanium (1582 K). Titanium correlates 1:1 with iron, consistent with both elements being entirely in refractory form. Removing a fraction of the dust from an accreting mass parcel lowers Fe and Ti in the same proportion. While ≈30% of disk-hosting A-type stars have a low surface abundance of these refractory elements (Folsom et al. 2012), among all A-type stars the fraction is only 2% (Gray & Corbally 1998; Paunzen 2001), confirming that

Table 2
Fundamental Stellar Parameters Relevant for Calculating the Photospheric Mixing Fraction, $f_{\rm ph}$, Following Jermyn & Kama (2018)

Star	$M_\star$ ($M_\odot$)	$R_\star$ ($R_\odot$)	$T_{\rm eff}$ (K)	$v_{\rm rot}$ (km s^{-1})	$\dot{M}$ ($M_\odot$ yr^{-1})	References
HD 31648	2.10 ± 0.25	1.9 ± 0.4	8800 ± 190	101.2 ± 1.7	$-6.95^{+0.12}_{-0.32}$	(1), (2)
HD 36112	2.8 ± 0.5	4 ± 1	8190 ± 150	57.8 ± 1.0	$-6.05^{+0.02}_{-0.03}$	(1), (3)
HD 68695	2.20 ± 0.15	1.9 ± 0.2	9000 ± 300	51 ± 4	$-7.78^{+0.38}_{-0.30}$	(1), (4)
HD 100546	2.3 ± 0.2	1.5 ± 0.3	10390 ± 600	64.9 ± 2.2	$-7.23^{+0.13}_{-0.13}$	(5), (7)
HD 101412	3.0 ± 0.3	4.2 ± 0.8	8600 ± 300	6.8 ± 0.4	$-7.04^{+0.15}_{-0.15}$	(1), (6)
HD 139614	1.7 ± 0.1	1.6 ± 0.4	7600 ± 300	25.6 ± 0.4	$-7.63^{+0.30}_{-0.20}$	(1), (4)
HD 141569	2.4 ± 0.2	2.0 ± 0.3	9800 ± 500	222 ± 7	$-7.65^{+0.47}_{-0.33}$	(1), (4)
HD 142666	1.95 ± 0.15	2.5 ± 0.3	7500 ± 200	68 ± 0.2	$-7.77^{+0.09}_{-0.12}$	(1), (3)
HD 144432	1.95 ± 0.20	2.6 ± 0.5	7400 ± 200	80.3 ± 1.0	$-7.74^{+0.09}_{-0.11}$	(1), (3)
HD 163296	2.3 ± 0.1	2.2 ± 0.2	9200 ± 300	122 ± 3	$-7.49^{+0.30}_{-0.14}$	(1), (4)
HD 169142	1.7 ± 0.2	1.9 ± 0.7	7500 ± 200	51.6 ± 0.5	$-8.70^{+0.13}_{-0.13}$	(1), (7)
HD 179218	3.1 ± 0.3	3.7 ± 0.6	9640 ± 250	70 ± 4	$-6.72^{+0.15}_{-0.24}$	(1), (3)
HD 244604	2.75 ± 0.40	3.6 ± 0.8	8700 ± 220	101 ± 5	$-7.2^{+0.26}_{-0.32}$	(1), (3)
HD 245185	2.3 ± 0.2	1.9 ± 0.4	9500 ± 750	136 ± 10	$-7.2^{+0.26}_{-0.32}$	(1), (3)
HD 278937	1.8 ± 0.1	1.7 ± 0.3	8000 ± 250	83.8 ± 4.6	$-6.66^{+0.15}_{-0.23}$	(1), (3)
T Ori	2.45 ± 0.15	3.1 ± 0.4	8500 ± 300	163 ± 11	$-6.58^{+0.40}_{-0.40}$	(1), (2)

References. (1) Folsom et al. (2012), (2) Mendigutía et al. (2011), (3) Donehew & Brittain (2011), (4) Fairlamb et al. (2015), (5) Kama et al. (2016), (6) Pogodin et al. (2012), (7) Wagner et al. (2015).

this is a short-lived surface contamination effect from disk accretion (Kama et al. 2015). Sulfur shows more scatter than titanium, but nonetheless displays a strong correlation with iron. This allows us to infer the fraction of sulfur locked in dust particles.

2.4. Refractory Fraction of an Element

We define $(\mathrm{X/H})_{\rm ref}$ as the reference abundance of element X in the material from which stars form, i.e., their bulk composition. This initial composition is mostly built up prior to the protoplanetary disk stage in which our disk hosts are and we assume it to be the same for the accreting, disk-hosting stars (sample stars) and nearby, young open cluster stars (reference stars) of the same effective temperature range (see also Appendix A). We determined the reference composition by taking an unweighted average of those open cluster stars for which a given element had been measured. Uncertainties on the open cluster reference abundances were calculated as the sample standard deviation, and these determine the size of the reference composition uncertainty ellipses in Figure 3.

We next define $f_{\rm X}$ as the fraction of X locked in refractories and $\delta_{\rm d}$ as the level of change of the refactory dust mass in the accretion stream, for example, due to a planet-induced dust cavity, where $\delta_{\rm d} < 1$ describes a depletion of dust and $\delta_{\rm d} > 1$ describes a dust excess. We assume the accretion stream composition directly samples the total elemental composition of the inner disk from which the stream originates. We then get the following for the abundance of X accreted from the disk onto the stellar photosphere:

$$\left(\frac{\rm X}{\rm H}\right)_{\rm disk} = [(1 - f_{\rm X}) + f_{\rm X}\ \delta_{\rm d}] \times \left(\frac{\rm X}{\rm H}\right)_{\rm ref}. \quad (1)$$

Now let $f_{\rm ph}$ be the mass fraction of accreted material in the photosphere of a star (Jermyn & Kama 2018). Then the observed stellar composition is related to the composition of the accreting material as

$$\left(\frac{\rm X}{\rm H}\right)_\star = f_{\rm ph}\left(\frac{\rm X}{\rm H}\right)_{\rm disk} + (1 - f_{\rm ph})\left(\frac{\rm X}{\rm H}\right)_{\rm ref}. \quad (2)$$

We determined $f_{\rm ph}$ using the methods in Jermyn & Kama (2018) for those stars with a measured accretion rate, rotational velocity $v \sin i$, and surface temperature. Equation (2) was then used to solve for the composition of the inner disk. Assuming $\delta_{\rm d}$, defined above as a dust mass scaling factor, affects the refractory component of all elements equally and thus cancels out, the accreted abundance of elements X and Y is related through

$$\left(\frac{\rm Y}{\rm H}\right)_{\rm disk} = \left(\frac{\rm Y}{\rm H}\right)_{\rm ref} \times \left[1 + \frac{f_{\rm Y}}{f_{\rm X}}\left(\frac{\left(\frac{\rm X}{\rm H}\right)_{\rm disk}}{\left(\frac{\rm X}{\rm H}\right)_{\rm ref}} - 1\right)\right]. \quad (3)$$

In our main analysis, we use the Bayesian Multinest sampling algorithm (Feroz & Hobson 2008; Feroz et al. 2009, 2013) to obtain posterior probability distributions on the free parameters, which are $f_{\rm S}$ and $f_{\rm Zn}$ globally, and $\delta_{\rm d}$ for each star. Zinc is excluded here due to a lack of good data as described in Appendix A, but see below for a tentative result on $f_{\rm Zn}$. We take uniform priors over $f_{\rm S}$ and $f_{\rm Na}$ from 0 to 1. We take a log-uniform prior for $\delta_{\rm d}$ from 10^{-3} to 10^{3}. Finally, we take the prior distribution of $f_{\rm ph}$ to be log-normal centered on the mean calculated computed using the methods in Jermyn & Kama (2018) and with variance determined by propagating uncertainties in the inputs to those methods. The resulting Gaussian is cut off at three standard deviations in each direction or at the logical boundary $f_{\rm ph} \leqslant 1$ of the domain, whichever is more restrictive. After sampling we marginalize over uncertainties in the accreted fraction $f_{\rm ph}$ and in the observed abundances.

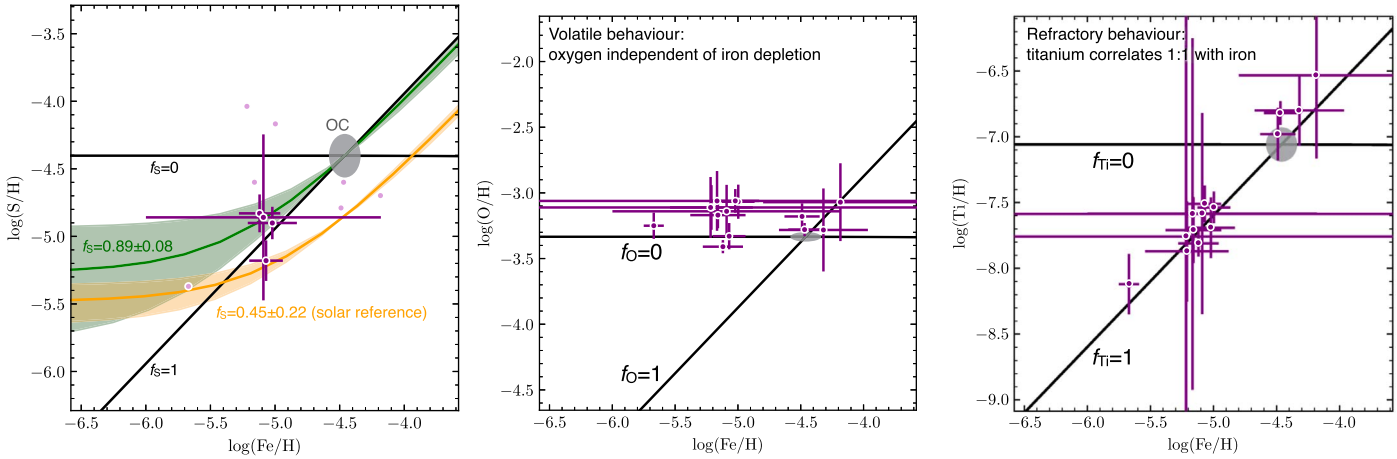

Figure 3. Abundance of sulfur (left-hand panel), oxygen (middle), and titanium (right-hand) vs. iron, normalized to hydrogen. For disk-hosting stars, the inferred composition of inner disk material is shown (dark purple). Stars with poorly quantified uncertainties were excluded (light purple, no errorbars shown). Errorbars include uncertainties on stellar parameters which factor into f_{ph}. The reference composition derived from open cluster data is defined to lie at the intersection of the 100% volatile and refractory behaviors ($f_X = 0$ and 1, solid black lines, "OC"). Our adopted fit uses the open cluster reference (green, 1σ shaded). A solar-reference fit (orange) is shown for comparison. See Appendix A for stellar composition references.

3. Results

We fit for the refractory fraction of O (which behaves essentially as a volatile), S, Zn, and Na. Elements with $T_c > 1000$ K are assumed to be entirely locked in dust and were assigned $f_X = 1$. This includes elements such as Fe, Mg, Si, and Ti. All uncertainties quoted below, and elsewhere in the paper, are given at 1σ.

We obtain $f_S = (89 \pm 8)\%$ for sulfur and $f_{Na} = (35 \pm 16)\%$ for sodium. This is the first measurement of the fraction of these elements locked in refractory reservoirs in protoplanetary disks. Note that we imposed no prior on the relation between f_S and f_{Na}. Equilibrium condensation calculations suggest $f_S < f_{Na}$, and imposing this constraint as a prior to check our results, we find $f_S = 89\%$ and $f_{Na} = 97\%$. This illustrates the robustness of our result for sulfur, and underlines the large uncertainty in f_{Na}.

We repeated this analysis using solar abundances from Asplund et al. (2009) as the stellar reference. Keeping in mind an unknown systematic offset from the early-type star abundances, this enabled us to also consider f_{Zn}, for which we took the prior to be uniform from 0 to 1. This yields $f_S = (45 \pm 22)\%$, $f_{Zn} = (52 \pm 34)\%$, and $f_{Na} = (77 \pm 18)\%$. The strong dependence of our results on the reference abundance points to the need to choose this from as similar a population of stars as possible. The increased uncertainty in these estimates relative to those from the field star reference reflects the generally worse fit obtained using the solar reference. This may also be seen in the Bayesian evidence, which was $\log L \approx -1401$ for the field star reference and $\log L \approx -9912$ for the solar reference. The two figures are not perfectly comparable because the solar reference enabled more elements to be used in the fit, which generally lowers $\log L$ by a factor of order the ratio of the number of observations used. This disagreement is much larger than that effect, though, because the solar abundance is not as reflective of the underlying bulk abundances of the open cluster A-type and young Herbig Ae/Be stars.

We carried out another check by performing orthogonal distance regression fitting of the sulfur–iron correlation, using solar abundances as the reference point. This yields a refractory sulfur fraction $f_S = (75 \pm 8)\%$, consistent with the Multinest results. Due to the self-consistent posteriors on the reference composition, we consider Multinest fitting with free reference values the superior approach and have highlighted the resulting f_S value $(89 \pm 8)\%$ as the most reliable.

The summarized statistics from our analysis are available on Zenodo in the Multinest JSON format, doi:10.5281/zenodo.3445366. The analysis methods were verified on test data, as discussed in Appendix B.

4. Discussion

4.1. Nature of the Sulfur Reservoirs

The high O abundance in all our accretion-contaminated stars points toward complete ice evaporation in, or prior to, the dust depletion location in the disks. At the H_2O snowline, any S-bearing volatile ices (H_2S, OCS, SO, and SO_2) would also have evaporated, enabling their gas-phase transport onto the central star. If there is significant refractory S, however, its trapping in the pressure bump would mean that material accreted to the star is S-poor, which is what we find.

This refractory sulfur must have a sublimation temperature higher than that of H_2O ($T_{sub} \approx 100$ K, Collings et al. 2004). This constraint is not met by the volatile species H_2S, CS, SO, and SO_2 which would all codesorb with water and accrete onto the star; but it is consistent with sulfide minerals, such as FeS ($T_{sub} \approx 655$ K—Larimer 1967; Lodders 2003) and with sulfur chains S_n, where $n = 2, \ldots, 8$. Sulfur chains are more volatile than sulfide minerals and experimentally less volatile than water (Jiménez-Escobar & Muñoz Caro 2011). According to these works, S_2 desorbs at $\gtrsim$150 K and S_3 at $\gtrsim$260 K. In contrast to efficient sulfide formation from gaseous H_2S and solid Fe (Lauretta et al. 1996); the abundance of stable sulfur chains only reaches $\lesssim$1% of all S nuclei in chemical models (Charnley 1997; Druard & Wakelam 2012) and ~6% in experiments (Jiménez-Escobar & Muñoz Caro 2011; Woods et al. 2015), adding to the weight of evidence favoring sulfide minerals as the main reservoir.

While cometary ices contain S_n at the percent level (Calmonte et al. 2016) and cometary dust is high in FeS content (Jessberger et al. 1988; Westphal et al. 2009), meteoritic rocks which sample inner solar system planetesimals show a mix of sulfides and chains: linear and cyclical sulfur chains intermixed with carbon

have a comparable abundance to that of sulfide minerals (Orthous-Daunay et al. 2010). The chain and sulfide groups together account for most of the meteoritic sulfur, although the relative abundances of various groups varies, perhaps due to a combination of different intrinsic abundances and parent body alteration history. We therefore favor the interpretation that the refractory S component in dust prior to incorporation in planetesimals is predominantly FeS and other sulfide minerals.

4.2. An Excess of Volatile Oxygen

Regardless of the level of depletion of the refractory elements Fe and Ti in disk-hosting stars, the O abundance does not vary. We find $f_{\rm O} = (2 \pm 2)\%$. This is low, as condensation models put $\sim$23% of O atoms in silicates (Lodders 2003), and warrants further study. Most oxygen occurs in volatile form in a solar-composition mixture (Lodders 2003). These considerations suggest that O is dominated by volatile carrier molecules and that the dust traps preventing refractories from accreting are always warm enough that the most abundant O-bearing ices—CO, CO_2, and H_2O—evaporate. The water snowline can be far out in the disks of these luminous stars. Detailed models of the HD 100546 disk show that H_2O ice can evaporate at the outer edge of its dust-depleted cavity, at $\sim$15 au (Kama et al. 2016). So a potential explanation to the apparent nondependence of oxygen on the level of dust depletion would be if higher levels of dust depletion correlated positively with an increased delivery of water molecules through the dust trapping region.

4.3. Longevity of Dust Traps and Stellar Abundance Anomalies

All of the disks around refractory-poor stars in our sample have dust-depleted regions in their inner disk on $\lesssim$10 au scales (Kama et al. 2015). The viscous spreading timescale[9] from 10 au is $t \sim 10^5$ yr, assuming the viscosity parameter is $\alpha = 10^{-2}$. Thus, the closer a dust-depleted zone is to the star, the more likely it is that the material currently observed to accrete onto the star has a physical memory of that particular zone. The stellar surface composition will change again on the viscous timescale if disk evolution alters the amount of dust reaching the star; or over $\sim 10^6$ yr after accretion stops, as diffusive mixing with deeper layers of the star dilutes away the chemical fingerprint of the surface layers (Turcotte & Charbonneau 1993; Jermyn & Kama 2018).

4.4. Implications for Exoplanets and the Solar System

Volatile and refractory sulfur reservoirs are observable in the products of planet formation: in solar system asteroids and comets, and in disrupted planetesimals around post-main-sequence stars (Figure 1, left-hand panel). The meteorites thought to most closely resemble primordial material from the inner 10 astronomical units of our protoplanetary disk are the CI chondrites (Wasson & Kallemeyn 1988). The S/Si ratio in these is very nearly equal to that in the Sun (Asplund et al. 2009). Meteorites such as CM or H chondrites that are fragments of processed, variably melted, differentiated parent bodies can have a substantially lower sulfur content. A similar, but larger range of sulfur abundance is inferred for exoplanetesimals accreting onto white dwarfs (Gänsicke et al. 2012; Xu et al. 2013, 2017), although the phase of sulfur in these bodies is uncertain and there may be measurement systematics as well as true initial abundance effects which push the highest inferred white dwarf planetesimal S/H ratio to a super-solar value (Figure 1).

The *Rosetta* spacecraft measured an elemental S/O ratio consistent with solar in both the ice and the dust of comet 67P/Churyumov–Gerasimenko (Calmonte et al. 2016, Figure 1). While cometary ices sample the volatile species of the outer disk, a significant fraction of the refractory cometary dust is thought to be reprocessed particles from the inner disk that were radially mixed outwards, based on their sulfide mineral content and the presence of crystalline silicates (e.g., Westphal et al. 2009). The high abundance of sulfur-bearing cometary ices suggests that sulfur was predominantly volatile at the onset of proto-solar disk formation, while its high abundance in rocky planetesimals supports the suggestion that sulfide minerals were produced in high abundance from H_2S or isomers of OCS reacting with solid Fe as the intensively accretion-heated inner few astronomical units of the proto-solar nebula cooled below 700 K (Haugen & Sterten 1971; Sterten & Haugen 1973; Kerridge 1976; Lauretta et al. 1996; Chambers 2009). Our measurement strongly supports such models, wherein the reprocessing of volatile sulfur species in disks to refractory minerals is a general process.

Differentiation of rocky planets such as Earth and Mercury is partly controlled by their sulfur content (Malavergne et al. 2014; Laurenz et al. 2016), and the element plays a major role in atmospheric chemistry and may have helped shield early life from ultraviolet radiation (Hapke & Nelson 1975; Winick & Stewart 1980; Kasting et al. 1989; Zhang et al. 2010). Our result provides a new constraint for protostellar and protoplanetary chemical models, and for observations tallying sulfur reservoirs in disks with ALMA and other submillimeter telescopes (Dutrey et al. 1997; Wakelam et al. 2004; Fuente et al. 2010; Dutrey et al. 2011; Martín-Doménech et al. 2016; Booth et al. 2018). We predict $\leqslant(11 \pm 8)\%$ of total sulfur in the gas and ice phases in the rocky planet formation zone of protoplanetary disks, which is predominantly further out than the $T_{\rm dust} \sim 700$ K destruction limit of FeS. If a large fraction of the refractory sulfur is in chains, the gas-phase sulfur abundance will be elevated above 11% at radii inwards of $\approx$200 K before peaking inside of 700 K.

In the near future, sulfur in the form of hydrogen sulfide (H_2S) may be observationally constrained in Hot Jupiter atmospheres with the *James Webb Space Telescope* (*JWST*) and other facilities. In the case of core accretion with a pure gas envelope, *JWST* may find very little H_2S in the atmospheres of Hot Jupiters, unless late accretion of planetesimals has provided significant contamination.

5. Conclusions

We have identified $(89 \pm 8)\%$ of all sulfur in refractory form in the innermost regions of protoplanetary disks. The main reservoir must be substantially more refractory than H_2O ice, which strongly favors sulfide minerals (e.g., FeS) over sulfur chain molecules (S_n). Almost all elemental sulfur is thus available for direct incorporation in rocky planetesimals in the inner few to 10 astronomical units around stars of $\approx$2 to 3 $M_\odot$. The rest is in volatile ices or gas-phase species.

This measurement was made possible by the use of accretion contamination on the surfaces of early-type stars as a probe of

[9] The viscous evolution timescale is $t_\nu = (\alpha\,\Omega_{\rm K})^{-1} \times (h/r)^{-2}$, where α is the Shakura-Sunyaev viscosity parameter, $\Omega_{\rm K}$ is the local Kepler time, and (h/r) is the scale height-to-radius ratio.

circumstellar material (Jermyn & Kama 2018). The radiative envelopes of such stars prevent recently accreted material from rapidly mixing with the deeper layers of the envelope, so the photospheric composition can easily be dominated by fresh material at accretion rates typical for protoplanetary disks.

The authors thank Ewine van Dishoeck for her useful comments on the manuscript. M.K. gratefully acknowledges funding from the European Union's Horizon 2020 research and innovation programme under the Marie Sklodowska-Curie Fellowship grant agreement No. 753799. A.S.J. is funded by the Gordon and Betty Moore Foundation through Grant GBMF7392 and the National Science Foundation under grant No. NSF PHY-1748958. K.F. is supported by JSPS KAKENHI grant No. 17K14245. C.W. acknowledges financial support from the University of Leeds and the Science and Technology Facilities Council (STFC; grant No. ST/R000549/1).

Appendix A
Data

A.1. Stars and Disks

Stellar elemental abundances for our analysis were taken from the studies of Folsom et al. (2012, Herbig Ae/Be stars), Kama et al. (2016 the Herbig Ae/Be star HD 100546), Fossati et al. (2011, NGC 5460), and Martin et al. (2017, NGC 6250). These studies used similar quality data and a similar methodology, whereby the stellar photospheric properties were determined simultaneously and self-consistently with the elemental abundances.

The Multinest fitting (Section 2.4) to obtain the refractory fractions $f_{\rm O}$, $f_{\rm S}$, $f_{\rm Zn}$, and $f_{\rm Na}$ was carried out globally over all stars and all elements, with a few exclusions. For each element–element combination, we excluded all stars for which a relevant abundance was determined from a single spectral feature and had an errorbar assigned from the researchers' experience as opposed to from spectral model fitting. We also entirely excluded open cluster stars with an effective temperature over 200 K away from the limits of the disk-hosting star sample. The excluded stars for sulfur (plotted as light-colored symbols without errorbars in Figure 3) were HD 31648, HD 36112, HD 68695, HD 179218, and HD 244604 in Folsom et al. (2012); and HD 123269, UCAC 11105213, and UCAC 11105379 in Fossati et al. (2011). Temperature excluded UCAC 12284506 in Martin et al. (2017). Mostly, the abundances of the excluded stars are 3σ-consistent with our final best fit. Finally, a sample study of abundances in Herbig Ae/Be stars by Acke & Waelkens (2004) which did include sulfur was excluded from consideration due to their different abundance-fitting methodology. These authors used stellar $T_{\rm eff}$, $R_\star$, and $\log(g)$ values from the literature and fitted only for the elemental abundances. A comparison of abundances for the stars in common between this study and that of Folsom et al. (2012) gives confidence that they are mostly within 3σ of each other.

The stellar parameters needed by the Jermyn & Kama (2018) formalism are summarized in Table 2, and the accretion stream (inner disk) compositions obtained by applying the resulting $f_{\rm ph}$ factor are given in Table 1.

The baseline abundance for each element was calculated as the mean of all open cluster stars which passed our exclusion criteria for that element, as described in the previous paragraph. We found solar abundances to be an unsatisfactory baseline for a number of elements, most likely due to a combination of Galactic chemical evolution in the $\sim$4 Gyr separating the young Sun from the birth of the relevant open cluster stars; and the different spectroscopic data and stellar models used to measure solar and early-type field star abundances.

A.2. Chondrites

We adopted the chondrite meteorite abundances from Wasson & Kallemeyn (1988). The most relevant here are the CI chondrites, which are thought to originate in undifferentiated, minimally processed parent bodies.

A.3. Comets

We adopt the S/O ratios measured for the volatile (evaporated ice) component of comet 67P/Churyumov–Gerasimenko by the ESA *Rosetta* mission, as reported in Calmonte et al. (2016). No other comet has yet been studied in comparable detail. The species included in the volatile S/O ratio calculation are H_2S, S, OCS, S_2, SO_2, SO, H_2O, CO, CO_2, and O_2. For the abundance of sulfur in the refractory dust of comet 1P/Halley, we use measurements from the PUMA mass-spectrometer (Jessberger et al. 1988) on Vega-1 (Sagdeev et al. 1986); and for comet 81P/Wild 2, X-ray spectroscopic measurements of a dust grain (Westphal et al. 2009) returned by the *Stardust* mission (Brownlee et al. 2006).

Appendix B
Testing

To verify our inference methods we generated an artificial data set composed of stars with depleted elemental abundances relative to solar abundances according to Equation (2). For these purposes different elements were assigned different refractory fractions and different stars were assigned different dust depletion factors. These abundances and the baseline were then contaminated with log-normal noise of various amplitudes. For each star a random subset of elements was dropped from the data set to reflect the fact that in actual observations not all elements have an abundance determination.

We performed our inference analysis on this artificial data set and were able to successfully infer the dust depletion factors as well as refractory fractions to within a tolerance of the same magnitude as the noise used to contaminate the sample.

ORCID iDs

Mihkel Kama https://orcid.org/0000-0003-0065-7267
Adam S. Jermyn https://orcid.org/0000-0001-5048-9973
Kenji Furuya https://orcid.org/0000-0002-2026-8157
Edwin A. Bergin https://orcid.org/0000-0003-4179-6394
Catherine Walsh https://orcid.org/0000-0001-6078-786X

References

Acke, B., & Waelkens, C. 2004, A&A, 427, 1009
Anderson, D. E., Bergin, E. A., Maret, S., & Wakelam, V. 2013, ApJ, 779, 141
Andrews, S. M., Huang, J., Pérez, L. M., et al. 2018, ApJL, 869, L41
Andrews, S. M., Wilner, D. J., Hughes, A. M., Qi, C., & Dullemond, C. P. 2009, ApJ, 700, 1502
Asplund, M., Grevesse, N., Sauval, A. J., & Scott, P. 2009, ARA&A, 47, 481
Birnstiel, T., Fang, M., & Johansen, A. 2016, SSRv, 205, 41
Boogert, A. C. A., Gerakines, P. A., & Whittet, D. C. B. 2015, ARA&A, 53, 541
Boogert, A. C. A., Schutte, W. A., Helmich, F. P., Tielens, A. G. G. M., & Wooden, D. H. 1997, A&A, 317, 929
Booth, A. S., Walsh, C., Kama, M., et al. 2018, A&A, 611, A16

Brownlee, D., Tsou, P., Aléon, J., et al. 2006, Sci, 314, 1711
Calmonte, U., Altwegg, K., Balsiger, H., et al. 2016, MNRAS, 462, S253
Chambers, J. E. 2009, ApJ, 705, 1206
Charnley, S. B. 1997, ApJ, 481, 396
Collings, M. P., Anderson, M. A., Chen, R., et al. 2004, MNRAS, 354, 1133
Danilovich, T., De Beck, E., Black, J. H., Olofsson, H., & Justtanont, K. 2016, A&A, 588, A119
Danilovich, T., Ramstedt, S., Gobrecht, D., et al. 2018, A&A, 617, A132
Danilovich, T., Van de Sande, M., De Beck, E., et al. 2017, A&A, 606, A124
Donehew, B., & Brittain, S. 2011, AJ, 141, 46
Druard, C., & Wakelam, V. 2012, MNRAS, 426, 354
Dutrey, A., Guilloteau, S., & Guelin, M. 1997, A&A, 317, L55
Dutrey, A., Wakelam, V., Boehler, Y., et al. 2011, A&A, 535, A104
Fairlamb, J. R., Oudmaijer, R. D., Mendigutía, I., Ilee, J. D., & van den Ancker, M. E. 2015, MNRAS, 453, 976
Feroz, F., & Hobson, M. P. 2008, MNRAS, 384, 449
Feroz, F., Hobson, M. P., & Bridges, M. 2009, MNRAS, 398, 1601
Feroz, F., Hobson, M. P., Cameron, E., & Pettitt, A. N. 2013, arXiv:1306.2144
Folsom, C. P., Bagnulo, S., Wade, G. A., et al. 2012, MNRAS, 422, 2072
Fossati, L., Folsom, C. P., Bagnulo, S., et al. 2011, MNRAS, 413, 1132
Fuente, A., Cernicharo, J., Agúndez, M., et al. 2010, A&A, 524, A19
Gänsicke, B. T., Koester, D., Farihi, J., et al. 2012, MNRAS, 424, 333
Geballe, T. R., Baas, F., Greenberg, J. M., & Schutte, W. 1985, A&A, 146, L6
Gray, R. O., & Corbally, C. J. 1998, AJ, 116, 2530
Hapke, B., & Nelson, R. 1975, JAtS, 32, 1212
Haugen, S., & Sterten, A. 1971, Oxidation of Metals, 3, 545
Hony, S., Bouwman, J., Keller, L. P., & Waters, L. B. F. M. 2002, A&A, 393, L103
Jenkins, E. B. 2009, ApJ, 700, 1299
Jermyn, A. S., & Kama, M. 2018, MNRAS, 476, 4418
Jessberger, E. K., Christoforidis, A., & Kissel, J. 1988, Natur, 332, 691
Jiménez-Escobar, A., & Muñoz Caro, G. M. 2011, A&A, 536, A91
Joseph, C. L., Snow, T. P., Jr., Seab, C. G., & Crutcher, R. M. 1986, ApJ, 309, 771
Kama, M., Bruderer, S., van Dishoeck, E. F., et al. 2016, A&A, 592, A83
Kama, M., Folsom, C. P., & Pinilla, P. 2015, A&A, 582, L10
Kasting, J. F., Zahnle, K., Pinto, J., & Young, A. 1989, OLEB, 19, 95
Keller, L. P., Hony, S., Bradley, J. P., et al. 2002, Natur, 417, 148
Keller, L. P., Rahman, Z., Hiroi, T., et al. 2013, LPSC, 44, 2404
Kerridge, J. F. 1976, Natur, 259, 189
Larimer, J. W. 1967, GeCoA, 31, 1215
Laurenz, V., Rubie, D. C., Frost, D. J., & Vogel, A. K. 2016, GeCoA, 194, 123
Lauretta, D. S., Kremser, D. T., & Fegley, B., Jr. 1996, Icar, 122, 288
Lisse, C. M., Kraemer, K. E., Nuth, J. A., Li, A., & Joswiak, D. 2007, Icar, 187, 69
Lodders, K. 2003, ApJ, 591, 1220
Malavergne, V., Cordier, P., Righter, K., et al. 2014, E&PSL, 394, 186
Martin, A. J., Stift, M. J., Fossati, L., et al. 2017, MNRAS, 466, 613
Martín-Doménech, R., Jiménez-Serra, I., Muñoz Caro, G. M., et al. 2016, A&A, 585, A112
Matsuura, M., Indebetouw, R., Woosley, S., et al. 2017, MNRAS, 469, 3347
Mendigutía, I., Calvet, N., Montesinos, B., et al. 2011, A&A, 535, A99
Orthous-Daunay, F.-R., Quirico, E., Lemelle, L., et al. 2010, E&PSL, 300, 321
Palumbo, M. E., Tielens, A. G. G. M., & Tokunaga, A. T. 1995, ApJ, 449, 674
Paunzen, E. 2001, A&A, 373, 633
Pinilla, P., Benisty, M., & Birnstiel, T. 2012, A&A, 545, A81
Pogodin, M. A., Hubrig, S., Yudin, R. V., et al. 2012, AN, 333, 594
Ryde, N., & Lambert, D. L. 2005, in ASP Conf. Ser.336, Cosmic Abundances as Records of Stellar Evolution and Nucleosynthesis, ed. T. G. Barnes, III & F. N. Bash (San Francisco, CA: ASP), 355
Sagdeev, R. Z., Blamont, J. E., Galeev, A. A., et al. 1986, SvAL, 12, 243
Semenov, D., Favre, C., Fedele, D., et al. 2018, A&A, 617, A28
Smith, R. G. 1991, MNRAS, 249, 172
Sterten, Å., & Haugen, S. 1973, Oxidation of Metals, 7, 45
Turcotte, S., & Charbonneau, P. 1993, ApJ, 413, 376
van der Marel, N., Verhaar, B. W., van Terwisga, S., et al. 2016, A&A, 592, A126
Wagner, K. R., Sitko, M. L., Grady, C. A., et al. 2015, ApJ, 798, 94
Wakelam, V., Caselli, P., Ceccarelli, C., Herbst, E., & Castets, A. 2004, A&A, 422, 159
Wasson, J. T., & Kallemeyn, G. W. 1988, RSPTA, 325, 535
Westphal, A. J., Fakra, S. C., Gainsforth, Z., et al. 2009, ApJ, 694, 18
Winick, J., & Stewart, A. 1980, JGRA, 85, 7849
Woods, P. M., Occhiogrosso, A., Viti, S., et al. 2015, MNRAS, 450, 1256
Woosley, S. E., & Weaver, T. A. 1995, ApJS, 101, 181
Xu, S., Jura, M., Klein, B., Koester, D., & Zuckerman, B. 2013, ApJ, 766, 132
Xu, S., Zuckerman, B., Dufour, P., et al. 2017, ApJL, 836, L7
Zhang, X., Liang, M.-C., Montmessin, F., et al. 2010, NatGe, 3, 834